Effects of fluoride salt addition to the physico-chemical properties of the $MgCl_2$-NaCl-KCl heat transfer fluid : a molecular dynamics study

Weiguang Zhou [a,c], Yanping Zhang [a,b,*], Mathieu Salanne [c,d,**]

[a] China-EU Institute for Clean and Renewable Energy, Huazhong University of Science & Technology, Wuhan 430074, China

[b] School of Energy and Power Engineering, Huazhong University of Science and Technology, Wuhan, China

[c] Sorbonne Université, CNRS, Physico-Chimie des Électrolytes et Nanosystèmes Interfaciaux, Paris, France

[d] Institut Universitaire de France (IUF), 75231 Paris Cedex 05, France

* Corresponding author. School of Energy and Power Engineering, Huazhong University of Science and Technology, Wuhan, China

** Corresponding author. Sorbonne Université, CNRS, Physico-Chimie des Électrolytes et Nanosystèmes Interfaciaux, Paris, France

E-mail address : zyp2817@hust.edu.cn (Y. Zhang), mathieu.salanne@sorbonne-universite.fr (M. Salanne)

Abstract

Concentrated solar plants are promising solutions for electricity production. In these plants, the heat transfer fluid plays an important role, and finding systems with good thermal properties is very important. In this regard, molten salts, and more particularly molten chlorides, are currently investigated. Experimental studies of these melts are difficult and expensive, so complementing them with simulations would allow to test a wider range of compositions. In this work, we show that classical molecular dynamics simulations are suitable for predicting the properties of a ternary salt composed of $MgCl_2$, KCl and NaCl by extensive comparisons with experimental data (and previous simulations) on the density, heat capacity, viscosity and thermal conductivity. We then

study the effect of adding fluoride ions in the melt on these properties in order to investigate the suitability of mixed chlorides-fluorides for future heat transfer fluids studies.

Keywords: Molecular dynamic simulation, Molten ternary chloride, Fluoride, Local structure, Thermodynamic properties

Nomenclature		H	enthalpy
V_{ij}	Interaction potential	k_B	Boltzmann constant
q_i, q_j	charge of ion	L_x, L_y, L_z	Cell length dimension in the x, y and z direction
r_{ij}	distance between particle i and j	ρ	density
B_{ij}, η_{ij}	BMH repulsive parameters	C_p	Specific heat capacity
C_{ij}, D_{ij}	Van der Waals parameters	μ	shear viscosity
$f_{dd}^{ij}, f_{dq}^{ij}, d_{dd}^{ij}, d_{dq}^{ij}$	Tang-Toennies parameters for Fumi-Tosi potential	λ	thermal conductivity
$f_n^{ij}, c_n^{ij}, b_n^{ij}, n$	Tang-Toennies parameters for polarization effects	J	heat flux
t	simulation time	$M(t)$	mean squared displacement
N	particle number	r_i	position of ion i
M	molar mass	D	self-diffusion coefficient
V	equilibrium volume	Subscripts	
N_A	Avogadro's constant	i, j, α, β	particle i, j, α, β
T	temperature	x, y, z	x, y, z dimension
P	pressure		

1. Introduction

Concentrated solar power (CSP) plant is a promising high-temperature solar power technology and is becoming one of the most massively planned solar power plant technology in the next few decades. An electricity generation target of 630 GW for CSP technology in 2050 is set by International Energy Agency (IEA)[1]. According to the US Department of Energy's sunshine initiative, increasing the competitiveness of CSP plants requires (1) increasing the operating temperature to

improve theoretical efficiency, and (2) effective thermal energy storage (TES) strategies to ensure dispatchability[2]. Currently, most CSP plants are equipped with TES system, so they can supply dispatchable and low-cost electricity with abundant but intermittent solar energy.

In a TES system, the heat transfer fluid (HTF) is particularly critical for overall performance and efficiency. The properties of an ideal HTF include: low melting point, high boiling point, thermal stability, low vapor pressure at high temperatures, low corrosion, low viscosity, high thermal conductivity, high specific heat capacity and low cost[3-5]. Molten salts are the most widely studied HTFs due to their good properties[6]. Molten nitrate salts are used in many large-scale current CSP plants, but they are limited to low temperatures, generally below 600℃[7, 8]. Nowadays, high-temperature CSP plants are developing, even exceeding 950℃[9]. Myers et al.[10] compared the data and concluded that chloride salts and their eutectics, such as the eutectic formed by the ternary system $MgCl_2$–NaCl–KCl (MNK), will be increasingly used in high-temperature TES system in CSP plants. It is therefore necessary to study the properties of molten chloride salts and their eutectics in the applications of HTF.

Molecular dynamics (MD) simulations have the advantages of low cost and high accuracy in acquiring the properties of molten salt at high temperature, while traditional experiments are costly and demanding. The main ingredient of these simulations is the interaction potential between the atoms, which can be estimated using an analytical force field (classical MD) or using first-principles electronic structure calculations, generally performed at the density functional theory (DFT) level (first-principles MD, FPMD). The latter being more accurate, it has been extensively been used to study molten chloride HTFs. Using this method, Liang et al.[11] studied the local structure and thermo-kinetic properties of pure molten magnesium chloride. Li et al.[12] unrevealed the thermophysical properties and microstructural evolution of MNK eutectic by comparing experimental measurements and FPMD simulations. Xu et al.[13] predicted the occurrence of structural transitions in the NaCl–$MgCl_2$ eutectic salt, which also provide insights for the applications of molten salts in TES system. Li et al.[14] studied the dynamic interaction of molten MNK with water impurity, which sheds insight for the development of salt purification technology. However, FPMD has a large computational cost, which could be avoided using classical MD. Simple molten chlorides, such as LiCl, NaCl, KCl and their mixtures have long been studied using the Born-Mayer-Huggins (BHM) potential[15], using the parameters proposed by Fumi and

Tosi[16]. Based on the same force field, Xie et al.[17] calculated the heat and mass transportation properties of LiCl–KCl and obtained results consistent with experimental literature data. However, the predictions may be improved by the use of polarizable force fields, such as the polarizable ion model (PIM) proposed by Madden and co-workers[18]. In the PIM, induced dipoles are introduced as additional degrees of freedom, which yields a better representation of complex ionic arrangements. Such force fields can be parameterized using DFT, ensuring a better transferability from one system to another[19]. Indeed, Wu et al.[20] investigated structural and thermodynamic properties of LiCl–NaCl–KCl system with different KCl concentrations by classical MD using either the BHM or the PIM force field and compared the results with reference FPMD calculations. They concluded that polarization effect increases the accuracy of the results. In parallel to the case of molten chlorides, PIM force fields were also developed for a large variety of molten fluorides[21]. Recently, new parameters were obtained for the $MgCl_2$ system and its mixtures with alkali chlorides[22], which was validated against X-ray scattering experiments[22,23]. This opens the door for the efficient simulation of HTFs based on this compound.

In this work, we first study the local structure and thermophysical properties of the MNK eutectic using PIM-based classical MD simulations. We then investigate the effect of additional fluoride ions, which are expected to deeply change the solvation shell of cations. The evaluated properties include radial distribution functions, density, specific heat capacity, self-diffusion coefficients, shear viscosity and thermal conductivity. All the simulations are performed under a wide range of temperatures. We have examined the precision of our MD simulation setup by comparing the simulated results for the ternary MNK with the available experimental data. After that, a small part of chloride ions in molten salt are replaced with fluoride ions, in order to compare and analyze the impact of fluoride ions on the local structure and thermophysical properties of molten salts.

2. Methodology

2.1 Force field

In this study, we use a pairwise additive force field, in which all the terms depend on the distance between the ions r_{ij}. It is given by:

$$V_{ij}\left(r_{ij}\right)=\frac{q_i q_j}{r_{ij}}+B_{ij}\exp\left(-\eta_{ij}r_{ij}\right)-f_{dd}^{ij}\left(r_{ij}\right)\frac{C_{ij}}{r_{ij}^{6}}-f_{dq}^{ij}\left(r_{ij}\right)\frac{D_{ij}}{r_{ij}^{8}}+f_{n}^{ij}\left(r_{ij}\right)\frac{q_j\mu_i\cdot r_{ij}}{r_{ij}^{3}} \quad (1)$$

The first term on the right side of Eq. (1) denotes the electrostatic interaction between ions. Then the second to fourth terms are Fumi-Tosi potential[16], in which the second term represents short-range repulsion force, while the third and fourth term describe dipole-dipole and dipole-quadrupole dispersion interactions respectively. Tang-Toennies functions[24] are used to damp the dispersion terms (third and fourth term) at short range:

$$f_{dd}^{ij}\left(r_{ij}\right)=1-\exp\left(-d_{dd}^{ij}r_{ij}\right)\sum_{k=0}^{6}\frac{\left(d_{dd}^{ij}r_{ij}\right)^{k}}{k!} \quad (2)$$

$$f_{dq}^{ij}\left(r_{ij}\right)=1-\exp\left(-d_{dq}^{ij}r_{ij}\right)\sum_{k=0}^{8}\frac{\left(d_{dq}^{ij}r_{ij}\right)^{k}}{k!} \quad (3)$$

All the parameters used in the Fumi-Tosi potential are listed in Table 1.

Table 1. Parameters of the Fumi-Tosi potential (all in atomic units) [23,25].

Pairs	η_{ij}	B_{ij}	C_{ij}	D_{ij}	d_{dd}^{ij}	d_{dq}^{ij}
Cl - Cl	1.797	275.1	140.0	280.0	1.7	1.7
Cl - Na	1.726	67.5	47.4	187.3	1.7	1.7
Na - Na	1.000	0.0	11.7	51.8	1.7	1.7
Cl - K	1.833	208.6	29.4	128.3	1.7	1.7
K - K	5.00	1.0	1.0	10.0	1.7	1.7
K - Mg	5.00	1.0	0.0	0.0	1.7	1.7
Mg - Mg	5.00	1.0	0.0	0.0	1.7	1.7
Cl - Mg	1.732	68.6	10.0	20.0	1.7	1.7
K - Na	5.00	1.0	0.0	0.0	1.7	1.7
Mg - Na	5.00	1.0	0.0	0.0	1.7	1.7
Cl - F	2.096	278.8	45.8	204.94	1.7	1.7
K - F	2.04	138.8	3.87	38.7	1.9	1.9
Na - F	1.974	52.83	13.25	88.15	1.9	1.9
Mg-F	1.938	45.58	13.25	88.15	1.9	1.9
F - F	2.44	282.3	15	150	1.9	1.9

The last term of Eq. (1) accounts for the polarization effects. Polarizable atoms carry an induced dipole μ_i interacting with all the point charges and all the other dipoles [18]. The influence of polarization effect on the structure and characteristics of molten salt should not be ignored, in particular in the presence of divalent species such as the Mg^{2+} cation[19]. As mentioned in the introduction, studies have shown that the results of molecular simulation considering the polarizable ion model are more robust than with the simpler BHM model[26]. The charge-dipole interactions are also damped at short-range with Tang-Toennies functions[24] defined as:

$$f_n^{ij}\left(r_{ij}\right)=1-c_n^{ij}\exp\left(-b_n^{ij}r_{ij}\right)\sum_{k=0}^{n}\frac{\left(b_n^{ij}r_{ij}\right)^k}{k!} \tag{4}$$

All the parameters of polarization term are listed in Table 2.[25]. The dipoles are calculated self-consistently at each timestep of the simulation using the conjugate gradient method, so that the polarization terms have a many-body character despite the pairwise additive form of the potential in Eq (1).

Table 2. Parameters for polarization term (all in atomic units). [c

charge	dipole	b_n^{ij}	n	c_n^{ij}	species	polarizability
Na	Cl	1.760	4	3.000	F	7.894
K	Cl	1.632	4	3.000		
Mg	Cl	1.873	4	2.875	Cl	20.000
Cl	Na	1.760	4	0.697		
F	Na	1.873	4	-0.190	Na	0.890
K	Na	1.760	4	0.000		
Mg	Na	1.760	4	0.000	Mg	2.000
Cl	K	1.632	4	0.917		
F	K	1.745	4	-0.310	K	4.717
Na	K	1.760	4	0.000		
Mg	K	1.760	4	0.000		
Na	F	1.837	4	2.543		
K	F	1.745	4	2.500		
Mg	F	1.918	4	1.858		

2.2 Simulation details

All simulations in this study are performed using the MetalWalls (MW) software [27], which is a MD code dedicated to the modelling of electrochemical systems. The simulation is divided into two groups, a first one labeled "base salt", which consists in the ternary $MgCl_2$–NaCl–KCl eutectic salts with a molar ratio of 45.37:32.96:21.67 mol%. The other salts include fluoride ions, that is they are made from the base salt in which 1% ,5%, 10% and 20% of chloride ions are replaced with fluoride ions. In the following they are labeled "MgNaKClF1%" , "MgNaKClF5%", "MgNaKClF10%" and "MgNaKClF20%" respectively. The corresponding atom numbers are provided in Table 3.

Table 3. Number of atoms for each simulated system

System		Na	K	Mg	Cl	F	Total
Base salt	**MgNaKCl**	**329**	**217**	**454**	**1454**	**-**	**2454**
Fluoride addition	**MgNaKClF1%**	**329**	**217**	**454**	**1439**	**15**	**2454**
	MgNaKClF5%	**329**	**217**	**454**	**1379**	**75**	**2454**
	MgNaKClF10%	**329**	**217**	**454**	**1304**	**150**	**2454**
	MgNaKClF20%	**329**	**217**	**454**	**1154**	**300**	**2454**

Also in each simulation, the periodic boundary conditions method is employed to keep constant the number of particles and eliminate boundary effects in the simulation box. The Ewald summation[28] method is used for long-range Coulomb potential as well as the charge-dipole and the dipole-dipole interactions. The velocity-Verlet algorithm is used to integrate the equations of motion in MetalWalls [29]. The experimental melting point of the ternary eutectic salts is about 656 K, so the preset temperatures are 800 K, 900 K, 1000 K, 1100 K and 1200 K for each system. Timestep for integrating the equations of motion is 0.5 fs. For all the simulations, the system are first simulated at ambient pressure in the NPT ensemble with Nosé–Hoover thermostat[30, 31] and barostat[32] at a constant pressure of 0.1 MPa for 500000 steps to reach equilibrium. After that, we keep the equilibrated system volume constant and simulate it in the NVT ensemble for at least 2000000 steps (1 ns). The relaxation times are 0.5 ps for the barostat and 0.1 ps for the thermostat.

2.3 Evaluated properties

2.3.1 Radial distribution functions

The local structures of molten salts is described by the partial radial distribution functions (RDF), which are defined as

$$g_{\alpha\beta}(r) = \frac{1}{4\pi\rho_{\beta} r^2}\left[\frac{dN_{\alpha\beta}(r)}{dr}\right] \tag{5}$$

where ρ_{β} is the number density of species β, $N_{\alpha\beta}(r)$ is the number of species β locating in a sphere with r as the radius and a specie α as the center.

In this work, all RDF data was calculated using TRAVIS [33] which is a program package for analyzing and visualizing molecular dynamics trajectories.

2.3.2 Density

Density is one of the critical properties of molten salt. It is defined as

$$\rho = \frac{NM}{VN_A} \tag{6}$$

Where N is the number of particles, M the molar mass and V the equilibrium volume of the system at given temperature and ambient pressure in the NPT ensemble simulations, and N_A is Avogadro's constant.

2.3.3 Specific heat capacity

Specific heat capacity is calculated as

$$C_p = \left(\frac{\partial H}{\partial T}\right)_p \approx \left(\frac{\Delta H}{\Delta T}\right) = \frac{\Delta(U + PV)}{\Delta T} \tag{7}$$

Where U is the total energy including kinetic energy and potential energy of the system. The variation of H is linear with respect to the temperature, so that C_p can be calculated from the slope of temperature enthalpy diagram of NPT simulations.

2.3.4 Shear viscosity

Shear viscosity (μ) is a critical property related to diffusion coefficients and structure, which partially determines the types of pipes and equipment used in the transportation and circulation of

HTFs in CSP. The shear viscosities are calculated in equilibrium MD using the Green-Kubo relationship. Specifically, they are obtained by time integration of the autocorrelation function of the stress tensor obtained by simulation [34] is given as follows,

$$\mu = \frac{V}{k_B T}\int_0^\infty \left\langle P_{xy}(0) P_{xy}(t) \right\rangle dt \tag{8}$$

Where k_B is Boltzmann constant and P_{xy} are the off-diagonal components of the stress tensor. In this study, there are five independent anisotropic components of the stress tensor, including $2zz - xx - yy, xx - yy, xy, xz$ and yz. Fig. 1 shows the autocorrelation function of these five stress tensor components for the MgNaKCl system at 1000 K as an example. It can be seen that each autocorrelation functions first decreases with time, and then fluctuates around 0, indicating that its time correlation has decayed. An average over the five components is made in order to improve the statistics. It is found that the integral of the integral of this averaged function reaches a plateau value after about 2 ps, even if the individual autocorrelation functions remained quite noisy. The viscosity is calculated from the value of this plateau. Note that 2 ps represents an estimate for the time scale of the structural relaxation of the system.

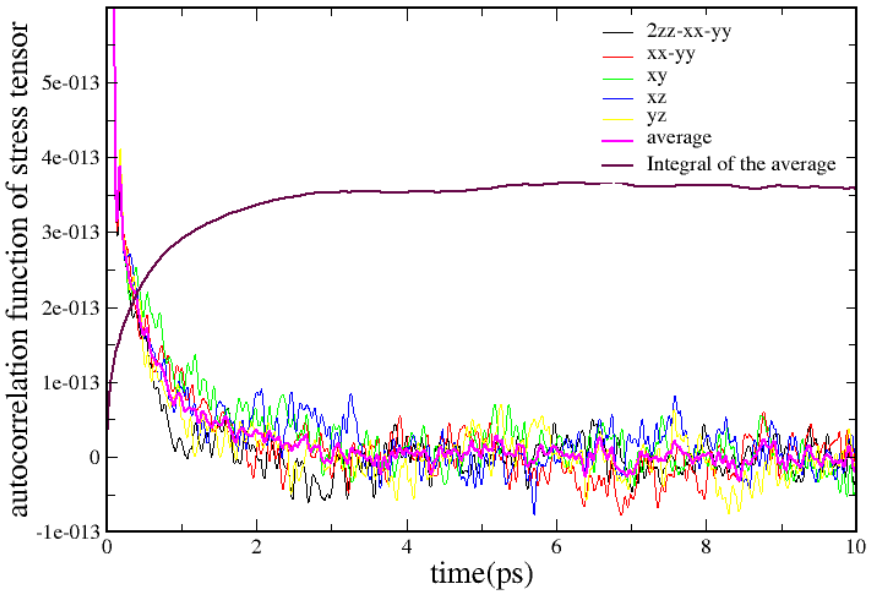

Figure 1. Stress tensor autocorrelation function of MgNaKCl simulation system at 1000 K. The viscosity is calculated by taking the value of the plateau of the integral.

2.3.5 Thermal conductivity

The thermal conductivity is calculated from Fourier's law using non-equilibrium MD (NEMD) method.

$$\lambda = -\frac{J}{\nabla T} \tag{9}$$

Where J is the heat flux and ∇T is the temperature gradient. The NEMD method calculates thermal conductivity by imposing a heat flux to the simulation box. As illustrated on Fig. 2, the simulation box is divided into 20 slices evenly along z-axis. The 1st slice is the hot region and 11th slice is the cold one. Because of the periodic boundary conditions, there are two resulting temperature gradients across the cell. Technically, this is achieved by modifying the particle velocity to increase or decrease a certain amount of energy in the two regions [35]. The temperature gradient ∇T is calculated from the average temperature of each slice. All the simulations start in the NVT ensemble until the system stabilizes at the set temperature. In a second step, the heat flux is imposed in NVE simulations for a total of 10^5 time steps to get the linear temperature gradient. Thermal conductivity is then calculated from Eq. (9).

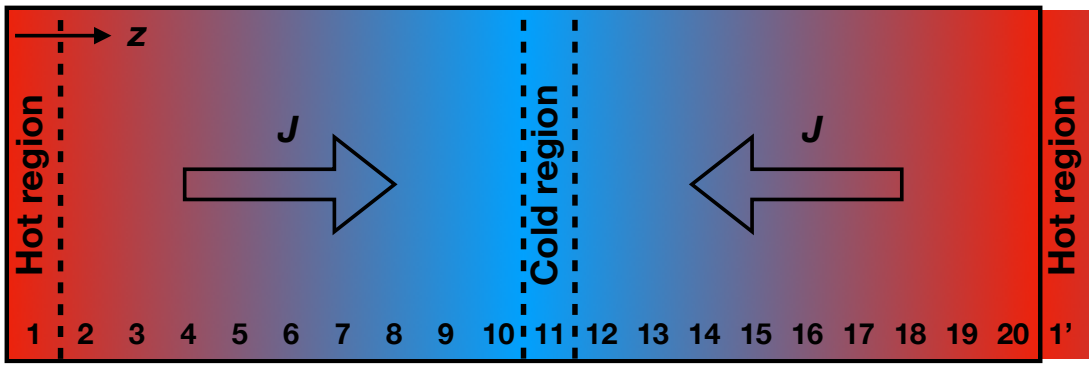

Figure 2. Schematic representation of the simulation box in the NEMD simulations. The box limits are shown with a thick line. The box is divided in 20 slices, the first one is defined as the hot region and the eleventh one as the cold region. Due to the periodic boundary conditions (slice 1' is the image of slice 1), there are two heat flux on the two sides of the cell [35].

2.3.6 Self-diffusion coefficient

The ion self-diffusion coefficient is calculated to study the transport properties of molten salt. In this work, they were calculated from time-dependent mean squared displacement (MSD) according to Einstein equation [34].

$$M(t)=\left\langle \left| r_i(t)-r_i(0) \right|^2 \right\rangle \tag{10}$$

$$D=\frac{1}{6}\frac{dM(t)}{dt} \tag{11}$$

Where the angle brackets <···> denotes ensemble average and r_i is the position of ion i.

3. Results and discussions

3.1 Base salt

In order to study the local structure of the chloride at different temperatures above the melting point, a series of partial radial distribution functions were calculated. Fig. 3 shows the RDF curves of the cation-anion pair and anion-anion pair in the MgNaKCl simulation system at 800 K. It can be seen that all RDF curves start from 0: because of the short-range repulsion, there is no other ions within the ionic radius of the ions. Then, all curves display a well-defined first peak which characterizes the short-range order. It is followed by a series of peaks which intensity gradually decreases with the distance; the RDFs progressively flatten and tend towards 1, which corresponds to the typical structure of molten salts [36].

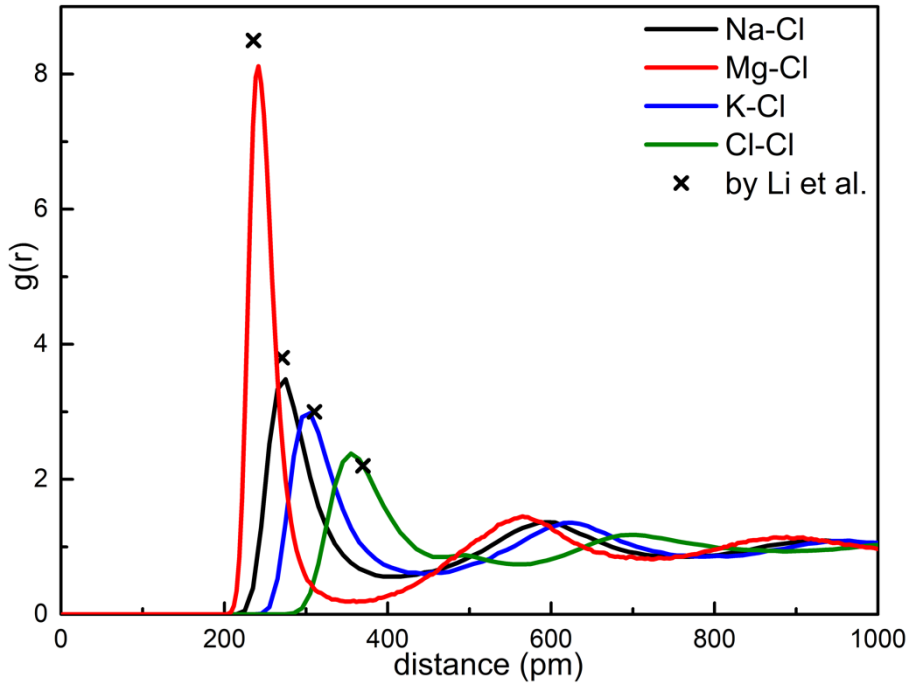

Figure 3. RDFs of cation-anion and anion-anion pairs at 800 K. The results are compared with FPMD simulations by Li et al. [12]

More specifically, Fig. 3 shows the RDFs of Na^+-Cl^-, K^+-Cl^-, Mg^{2+}-Cl^- and Cl^--Cl^- ion pairs at 800 K. It can be seen the first peak of Mg^{2+}-Cl^- is significantly higher than that of Na^+-Cl^- and K^+-Cl^-, because of the stronger interaction between Mg^{2+}-Cl^- ion pairs. The first peak positions of each ion pair from FPMD simulation by Li et al. [12] are also marked in Fig. 3. In all cases the agreement is good for both the positions and the heights of the peaks, showing the ability of the PIM-based classical simulations to predict the correct structure of the melt.

Fig. 4 shows RDFs of Na^+-Cl^-, Mg^{2+}-Cl^-, K^+-Cl^- and Cl^--Cl^- ion pairs at different temperatures. It can be seen from the partial enlarged view of the peak that as the temperature increases, the height of the peak decreases, which is due to the decrease of the density. Moreover, it can be found that the positions of the first peaks of these three cation-anion pairs are slightly shifted leftward as the temperature increases, which means that the distance between anion and cation becomes shorter at high temperatures. However, there is a slight shift to the right for the anion-anion pairs, which indicates that the distance between the ion clusters increases at high temperatures.

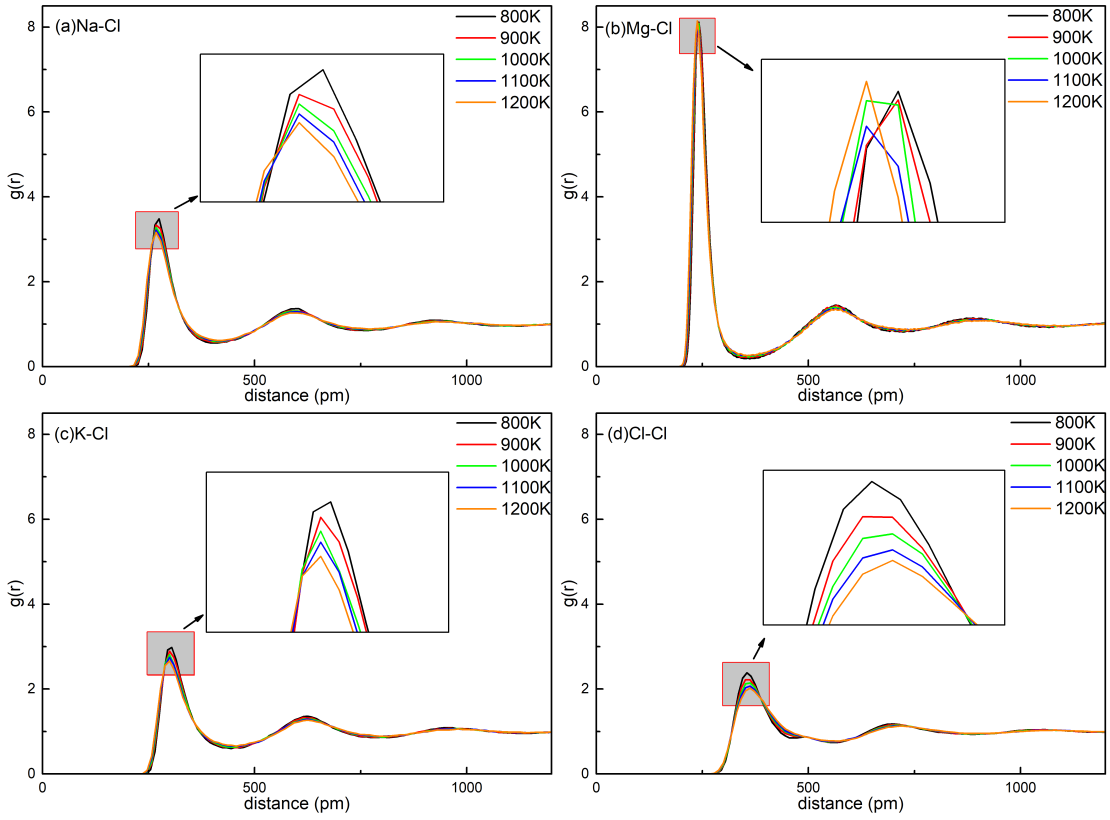

Figure 4. RDFs of cation-anion and anion-anion pairs at each temperature

In Fig. 5, the densities of the base salt (MgNaKCl) calculated from the NPT simulations are compared with the experimental results obtained for the same composition by Li et al.[12].

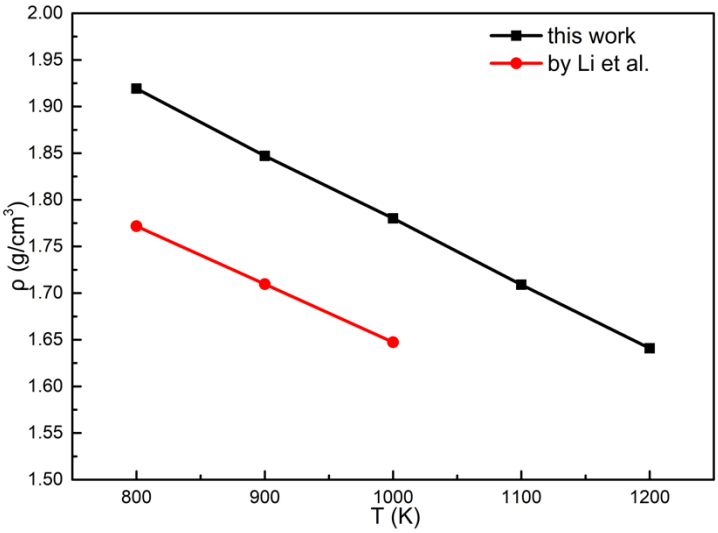

Figure 5. Temperature dependence of density for MgNaKCl. The simulation results are compared with experiments for the same composition from Li et al. [12].

Obviously, density and temperature are negatively correlated linearly. The densities decrease from $1.92\ \mathrm{g/cm^3}$ to $1.64\ \mathrm{g/cm^3}$ with an increase in temperature from 800 K to 1200 K. A linear fit of our results yield the following relationship.

$$\rho_{MgNaKCl}=2.4794 - 0.7\times10^{-3}T \tag{12}$$

The simulation results are slightly larger than the experimental results, and the overall deviation is 8.14%, which may be due to the fact that the force field parameters were derived from DFT calculations, and are not empirical [23,25]. Indeed, despite the intrinsically more accurate character of FPMD, Li et al. obtained similar level of agreement with the experimental density in their previous study [12].

Fig. 6 shows the temperature variation enthalpy of the MgNaKCl system, obtained from the NPT simulations. The enthalpy varies linearly, which shows that the specific heat capacity is nearly constant among the whole temperature range based on equation (7). It is worth noting that some discrepancies are observed among experimental results about such a trend. In recent studies (on different salt compositions), Wang et al. reported changes of the heat capacity with temperature [37], while Xu et al. did not observe such a variation [38]. In their review of the literature, Villada et al. showed that the latter behavior is more common, in agreement with our results [39]. The calculated specific heat capacity of MgNaKCl is $1.09\ \mathrm{J/(g\cdot K)}$, is in good agreement compared with the experimental result of $1.14\ \mathrm{J/(g\cdot K)}$ by Li et al.[12] with a deviation of 4.4%.

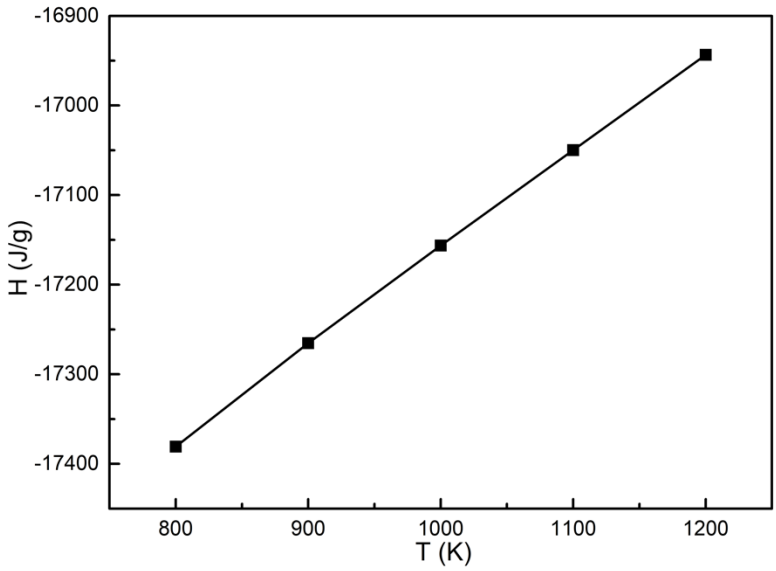

Figure 6. Variation of the calculated enthalpy with temperature for the base salt.

As shown in Fig. 7, the viscosity of the system decreases sharply as the temperature rises. Although no available experimental data on the viscosity of our studied composition in the literature, we compare the simulation results to the ones on $MgCl_2$-NaCl-KCl (50-30-20 mol.%) by Li et al.[40] and $MgCl_2$-NaCl-KCl (47.1-30.2-22.7 mol.%) by Villada et al. [39]. Considering the different compositions of the molten salt, the agreement is good, except for the lowest studied temperature at which the predicted viscosity is too large.

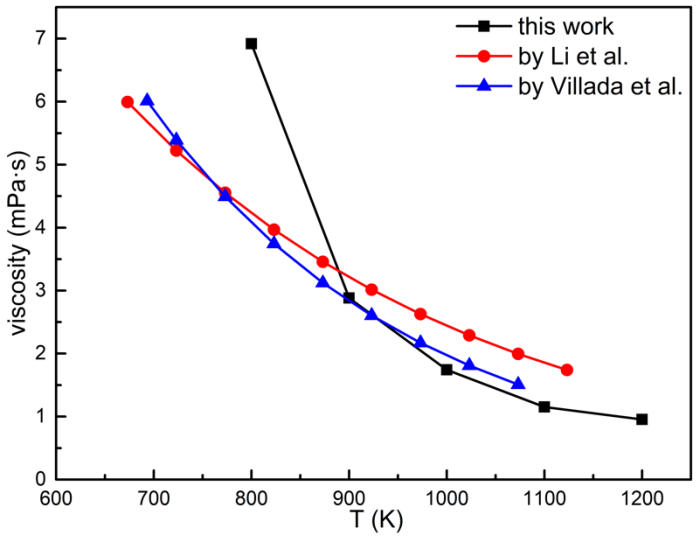

Figure 7. Viscosity of MgNaKCl system of $MgCl_2$-NaCl-KCl. The simulation results are compared with the data of Li et al. [40] and Villada et al. [39] (obtained on different salt compositions).

For the NEMD calculation of the thermal conductivity, parallelepipedal simulation cells were generated by replicating several times the initial cubic cell along the *z*-axis. We performed several tests in which the simulation cell was replicated between 2 and 6 times. They yielded similar results, so that the cell with $L_z = 2\ L_x$ was further chosen in order to keep a low computational cost. The

temperature profiles obtained for MgNaKCl with an applied heat flux of $2.32 \times 10^{-10}\,\mathrm{W/Å^2}$ at each temperature are plotted in Fig. 8. A linear variation is observed between the hot region and the cold region.

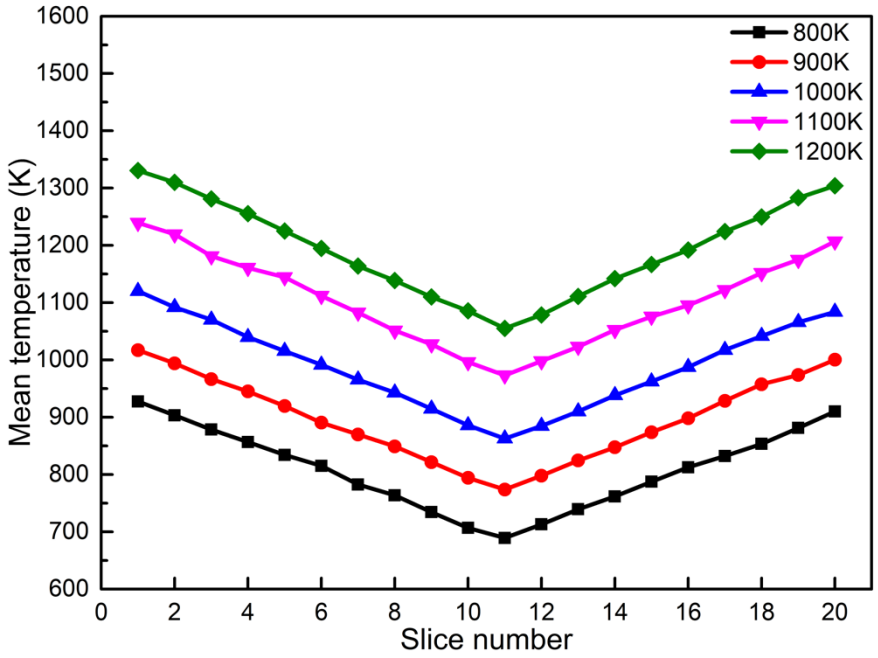

Figure 8. Mean temperature profile along the simulation cell at each imposed temperature

The slopes of the temperature variation along the *z* dimension were extracted in order to compute the thermal conductivity of the system according to Eq. (9). As shown in Fig. 9, the thermal conductivity of MgNaKCl decreases with temperature, from $0.44\,\mathrm{W/K \cdot m}$ at 800K to $0.36\,\mathrm{W/K \cdot m}$ at 1200K. As for the viscosity, experimental data on this specific MgNaKCl composition is lacking. We thus compare the simulation results with the measurements of Wang et al. [37] for a (45.98%-15.11%-38.91% mol) composition; a good overall agreement is obtained. Villada et al. [39] also tried to estimate the conductivity of the (47.1-30.2-22.7 mol.%) composition using a linear mixing rule and the values provided in the literature for the pure salts (NaCl and KCl by Nagasaka et al.[41], $MgCl_2$ by Lu et al.[26]). Their results are slightly overestimated, which may be due to the use of mixing rule. As was demonstrated from simulations of binary molten fluorides [42], the mixtures systematically display lower values for the thermal conductivity than pure salts.

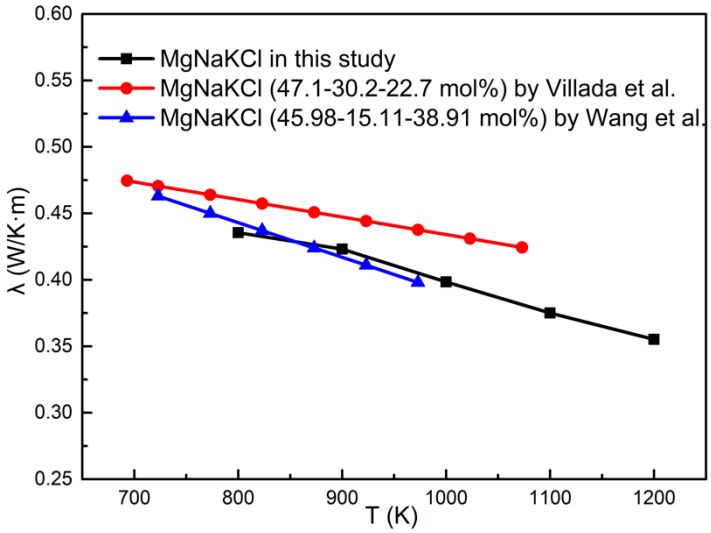

Figure 9. Thermal conductivities of MgNaKCl system in different temperature. Results are compared with experimental results by Wang et al. [37] and Villada et al. [39]

Fig. 10 shows the linear relationship between the MSD of each ion and time at 1000 K. According to Eq. (11), the diffusion coefficient of each ion at each temperature is calculated by the slope. It can be found that the order of the diffusion coefficient of each ion is $D_{Na^+} > D_{K^+} > D_{Cl^-} > D_{Mg^{2+}}$ in Fig. 11, which is affected by the mass, ionic radius, the number of charges and ion interaction. As far as we know, there are few studies on the self-diffusion coefficient of ternary $MgCl_2$–NaCl–KCl molten salts, but by comparing with the experimental data of NaCl by Janz [43] , the experimental data of KCl by Bockris et al. [44] and the FPMD data of $MgCl_2$ by Liang et al.[11] , the differences are small and the trend is consistent.

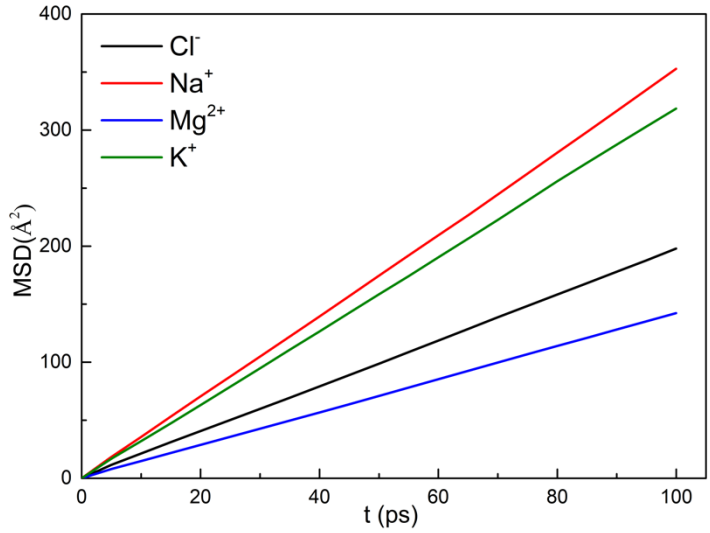

Figure 10. MSD of each ion in MgNaKCl system at 1000 K

Fig. 11 shows that the self-diffusion coefficient increases with increasing temperature, which means

that the movement of ions will be easier. This agrees with previous result: as the temperature rises, the structure of the molten salt becomes loose and diffusion becomes easier. The self-diffusion coefficient of divalent cation Mg^{2+} is smaller than those of monovalent species due to the stronger Mg^{2+}-Cl^- interaction.

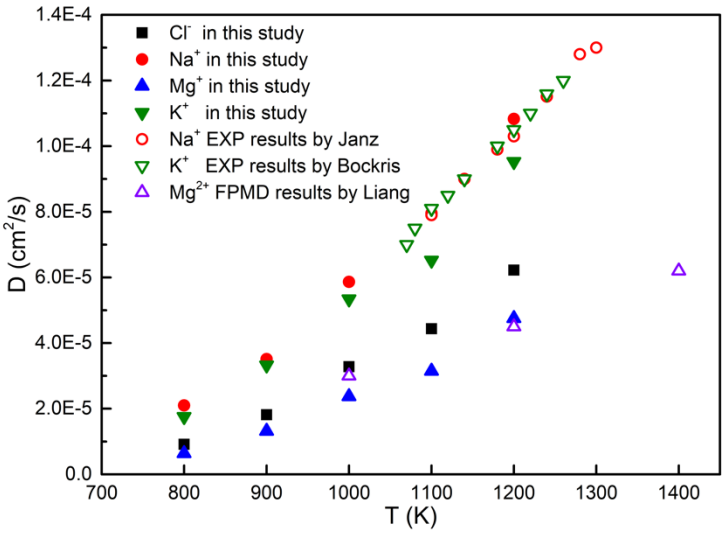

Figure 11. Self-diffusion coefficient of each ions in MgNaKCl systems in different temperature. The results are compared with previous experimental (Janz [43], Bockris [44]) and FPMD (Liang [11]) studies on the pure salts.

3.2 Effect of Fluoride salt addition

Since the computed properties on the ternary molten chloride are in agreement with experimental data, it is possible to make predictions on new salt compositions. In this study, four systems were simulated, in which 1%, 5%, 10% and 20% of the chloride ions of the base salt were replaced by fluoride ions to study their effect on the local structure and thermodynamic properties.

For the local structure, the RDFs of cation-anion and anion-anion pairs are shown in Fig. 12. At first sight, the interactions seem to be stronger for the Na^+-Cl^- pair than for the Na^+-F^- one. A similar effect is observed for K^+-Cl^- and K^+-F^-. On the contrary, there is stronger interaction between Mg^{2+}-F^- than Mg^{2+}-Cl^-. These observations can therefore be rationalized by the fact that the Mg ion attracts more fluoride ions in its vicinity due to its divalent character, which explains the depletion of the latter in the solvation shell of Na^+ and K^+.

For anion-anion pairs, the Cl^--F^- nearest-neighbor distance is shorter than the Cl^--Cl^- one, which is

due to the smaller radius of F^-. This indicates that the distance between the ion clusters becomes smaller upon addition of F^- , and thus the system volume will be smaller, which can impact the density. The smaller distance between the ion clusters may also lead to larger shear viscosity.

As the proportion of fluoride ions increases, the height of the peak between Na^+-$Cl^-$and K^+-Cl^- gradually increases, while the one of the Mg^{2+}-Cl^- RDF gradually decreases. In contrast, as the proportion of F^- increases, the interaction between Na^+-F^- and K^+-F^- gradually decreases, while the Mg^{2+}-F^- one gradually increases. Again, the main reason for this difference is that the interaction between Mg^{2+} and F^- is very strong, so as the proportion of F^- increases, more Mg^{2+} will surround F^-, and the extra vacancies around Cl^- will naturally be occupied by Na^+ and K^+ cations.

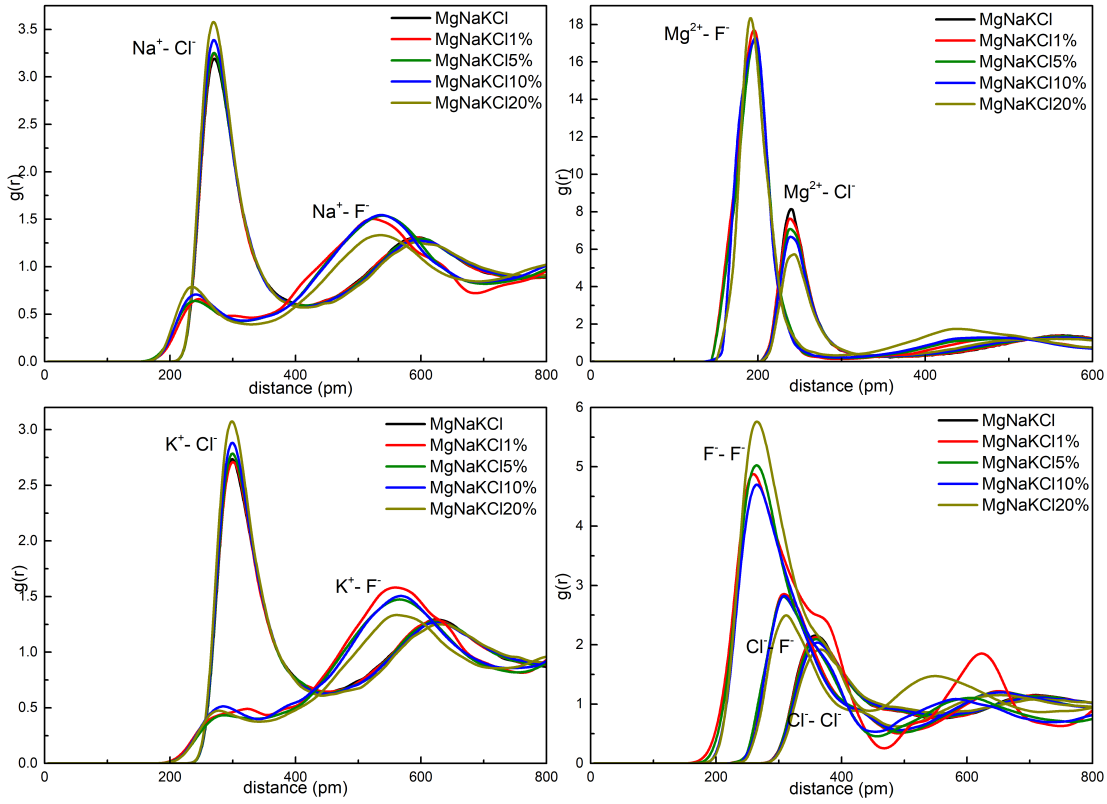

Figure 12.RDFs of cation-anion and anion-anion pairs for the fluoride ion containing systems

We now analyze variations in the density. Fig. 13 shows the density of each system at 1000 K. We observe that replacing part of the chloride ions in MgNaKCl with fluoride ions leads to an increase of the density. The greater the proportion of fluoride, the greater the increase in density; the 20% fluoride system leads to an increase of the density from 1.78 g/cm^3 to 1.84 g/cm^3 with respect to the base salt. However, comparing the molar mass of chlorine and fluorine, Cl > F, so the overall mass of the system decreases as the replacement ratio increases. The reason for the increase in

density must be related to changes in its volume and structure. From the previous RDFs analysis, the relatively strong interactions of Mg^{2+}-F^- pair makes the main contribution to volume reduction and structural changes of the system.

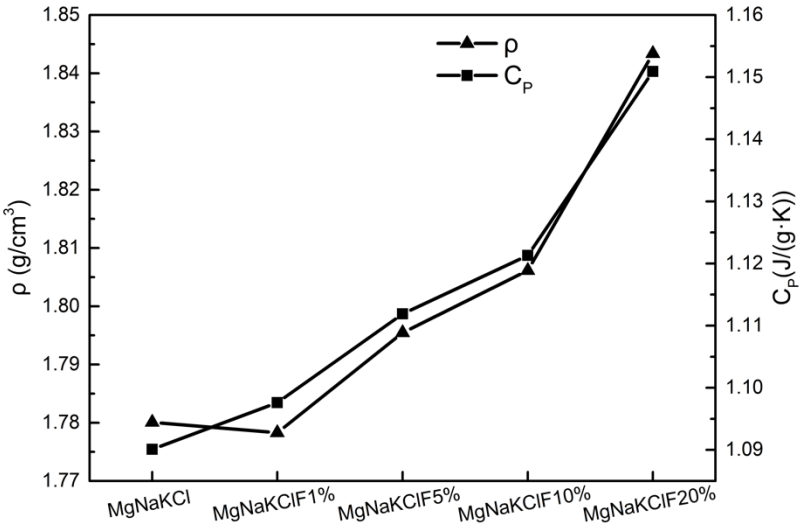

Figure 13. Density (at 1000K) and specific heat capacity of each simulated systems

For specific heat capacity (C_P), the results are 1.0976 $J/(g \cdot K)$, 1.1119 $J/(g \cdot K)$, 1.1213 $J/(g \cdot K)$ and 1.1509 $J/(g \cdot K)$ for MgNaKClF1%, MgNaKClF5%, MgNaKClF10% and MgNaKClF20%, respectively. Fig. 13 shows the specific heat capacity of each simulated systems. Obviously, the adding of fluoride ions leads to an increase oof the C_P of the salt, and the larger the proportion of fluoride ion, the more C_P increases. Specific heat capacity increased by 0.69%, 2.00%, 2.86% and 5.58% respectively. As shown on Fig. 13, this change in the specific density is well correlated with the corresponding density increase with composition.

For viscosity, Fig. 14 shows that the influence of the concentration in fluoride ion is not monotonous; it appears that the effect is important at large concentration only. In addition, at high temperature, the fluoride ion addition has a smaller effect on the viscosity. Note however that the uncertainty on the calculation of the viscosity is relatively large, which may explain the absence of a clear trend with concentration.

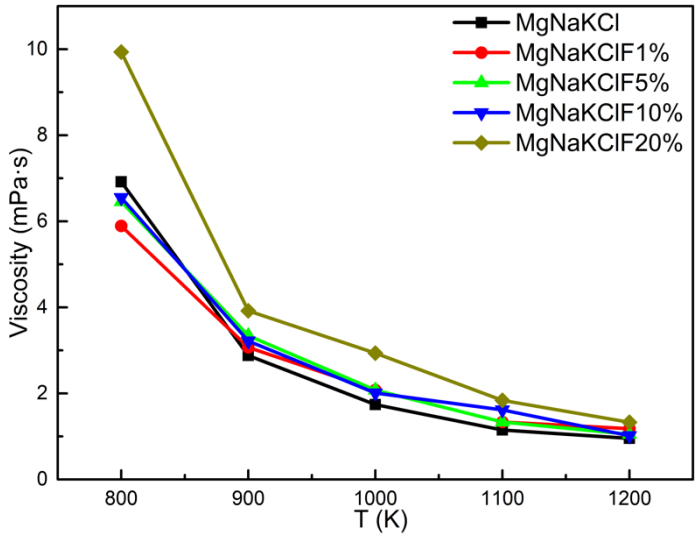

Figure 14. viscosity of each simulated systems at each temperatures

For thermal conductivity, Fig. 15 shows that the thermal conductivities of the three systems all decrease with increasing temperature. As the proportion of fluoride ions increases, the thermal conductivity of the system increases. The main reason is that the volume of the system becomes smaller, so that the heat transfer between the ions becomes easier. Compared with MgNaKCl, the thermal conductivity of MgNaKClF1%, MgNaKClF5%, MgNaKClF10% and MgNaKClF20% each have an average increase of 1.21% and 5.27%, 5.79% and 13.36%.

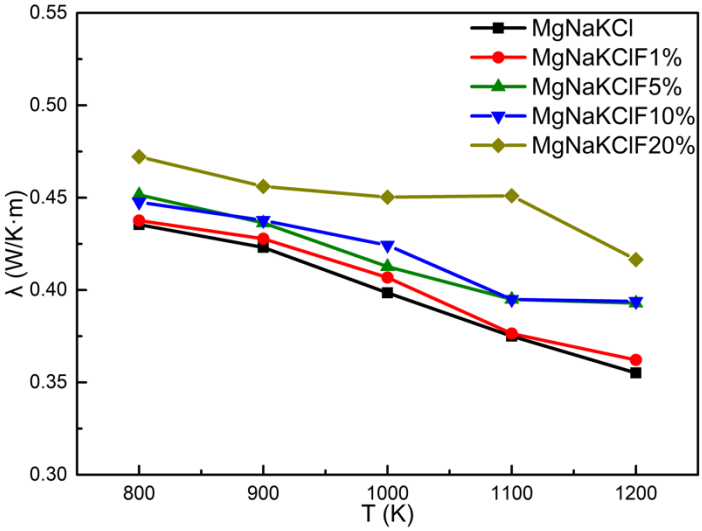

Figure 15. Thermal conductivity of each simulated systems on the whole range of temperatures

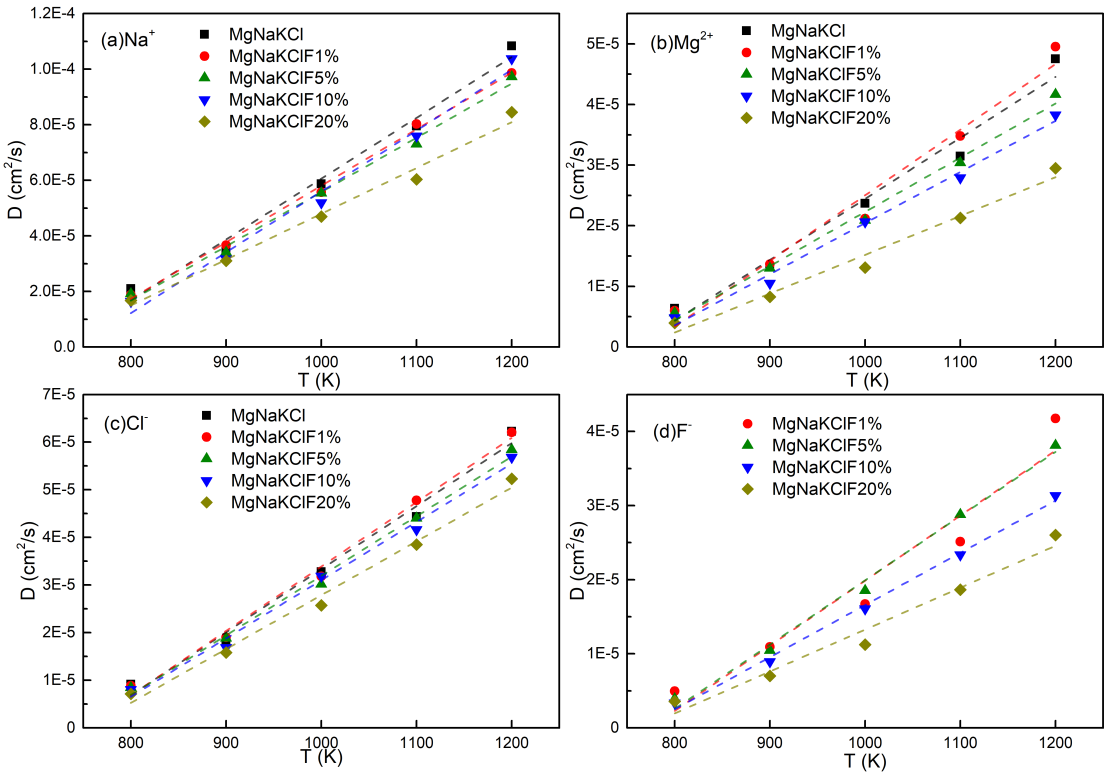

Figure 16. Diffusion coefficients of (a) Na^+, (b) Mg^{2+}, (c) Cl^-, (d) F^- in the five systems over the whole range of studied temperatures.

Finally, Fig. 16 shows the diffusion coefficient of each particles at each temperature for the five systems. Consistent with the previous discussion, the self-diffusion coefficient of each particle in each system increases as the temperature rises. Fig. 17 shows the self-diffusion coefficients of the particles in the 5 different systems at 1000 K. It can be seen that as the proportion of fluoride ions increases, the self-diffusion coefficient of each particle generally decreases, but it is not monotonous. The decrease is more pronounced at high temperatures. The impact of fluoride ion concentration on the various ions is also different. At 1200 K, the self-diffusion coefficient of Mg^{2+}, Na^+ and K^+ decreased by 37.99%, 21.95% and 10.97% in the MgNaKClF20% system.

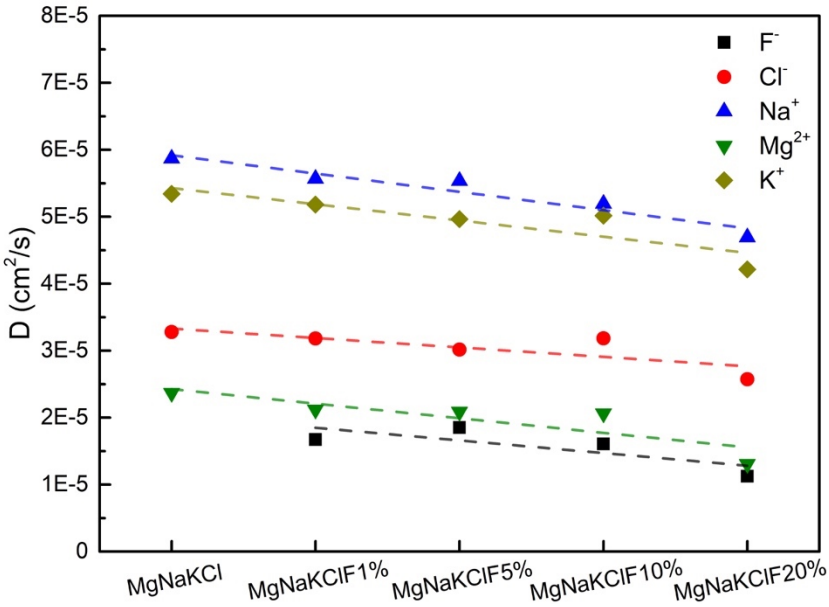

Figure 17. Self-diffusion coefficient of each particles at 1000K in different systems

4. Conclusions

In this study, we performed classical MD simulation of the ternary chloride salt $MgCl_2$–NaCl–KCl with and without additional fluoride anions. The interactions are represented using the PIM model, which includes explicitly polarization effects in the force field. The local structure, thermodynamic and transport properties (radial distribution function, density, specific heat capacity, viscosity, thermal conductivity, and self-diffusion coefficients) of the molten salt were obtained in order to evaluate the performance of the salts as HTF in CSP.

For the base salt system, by comparing our simulations with the experimental results in the literature, we showed that the selected force field accounts properly for the interactions of the ternary chloride salt. The temperature dependence of each properties were determined. In a second step, this study discusses the effect of adding fluoride ions on the evaluated properties. In terms of local structure, changes are mainly due to the strong interaction between Mg^{2+}-F^-, which leads to more F^- in the solvation shell of Mg^{2+} instead of Cl^-. From the perspective of HTF application, high specific heat capacity, low shear viscosity and high thermal conductivity are more important in the selected properties. The addition of fluoride ion is very beneficial to increase the specific heat capacity and thermal conductivity of the molten salt. 20% fluoride addition leads to a specific heat increase of 5.58% and an average thermal conductivity increase of 13.36%. However, the addition of fluoride

salt also leads to a higher viscosity. Using this strategy for enhancing HTFs would therefore need to select the best compromise between the various target properties. It should be noted that the phase diagram of the mixed chloride-fluoride salts are not known, which would be a necessary step before a practical application of such salts in HTFs.

Declaration of competing interest

The authors declare that they have no known competing financial interests or personal relationships that could have appeared to influence the work reported in this paper.

CRediT authorship contribution statement

Weiguang Zhou: Methodology, Software, Validation, Investigation, Data curation, Visualization, Writing – original draft. **Yanping Zhang**: Supervision, Writing – review & editing. **Mathieu Salanne**: Conceptualization, Software, Methodology, Writing – review & editing, Supervision, Project administration, Funding acquisition.

Acknowledgments

The authors acknowledge HPC resources granted by the HPCaVe Centre at Sorbonne Université.

Data availability

The data generated within this study are available on Zenodo at the following address: http://dx.doi.org/10.5281/zenodo.5045186.

References

[1] S. Guillot, A. Faik, A. Rakhmatullin, J. Lambert, E. Veron, P. Echegut, C. Bessada, N. Calvet, X. Py, Corrosion effects between molten salts and thermal storage material for concentrated solar power plants, Applied Energy, 94 (2012) 174-181.
[2] W. Ding, T. Bauer, Progress in Research and Development of Molten Chloride Salt Technology for Next Generation Concentrated Solar Power Plants, Engineering, 7 (2021) 334-347.
[3] K. Vignarooban, X. Xu, A. Arvay, K. Hsu, A.M. Kannan, Heat transfer fluids for concentrating solar power systems – A review, Applied Energy, 146 (2015) 383-396.
[4] J. Pacio, T. Wetzel, Assessment of liquid metal technology status and research paths for their use as efficient heat transfer fluids in solar central receiver systems, Solar Energy, 93 (2013) 11-22.
[5] J.G. Cordaro, N.C. Rubin, R.W. Bradshaw, Multicomponent molten salt mixtures based on nitrate/nitrite anions, Journal of Solar Energy Engineering, 133 (2011).

[6] Q. Peng, J. Ding, X. Wei, J. Yang, X. Yang, The preparation and properties of multi-component molten salts, Applied Energy, 87 (2010) 2812-2817.
[7] U. Herrmann, D.W. Kearney, Survey of Thermal Energy Storage for Parabolic Trough Power Plants, Journal of Solar Energy Engineering, 124 (2002) 145-152.
[8] K.H. Stern, High Temperature Properties and Decomposition of Inorganic Salts Part 3, Nitrates and Nitrites, Journal of Physical and Chemical Reference Data, 1 (1972) 747-772.
[9] B. Hoffschmidt, F.l.M. Te´llez, A. Valverde , J.s. Ferna´ndez , V. Ferna´ndez, Performance Evaluation of the 200-kWth HiTRec-II Open Volumetric Air Receiver, Journal of Solar Energy Engineering, 125 (2003) 87-94.
[10] P.D. Myers, D.Y. Goswami, Thermal energy storage using chloride salts and their eutectics, Applied Thermal Engineering, 109 (2016) 889-900.
[11] W. Liang, J. Wu, H. Ni, G. Lu, J. Yu, First-principles molecular dynamics simulations on the local structure and thermo-kinetic properties of molten magnesium chloride, Journal of Molecular Liquids, 298 (2020).
[12] X. Li, N. Li, W. Liu, Z. Tang, J. Wang, Unrevealing the thermophysical properties and microstructural evolution of MgCl2–NaCl–KCl eutectic: FPMD simulations and experimental measurements, Solar Energy Materials and Solar Cells, 210 (2020).
[13] T. Xu, X. Li, L. Guo, F. Wang, Z. Tang, Powerful predictability of FPMD simulations for the phase transition behavior of NaCl-MgCl2 eutectic salt, Solar Energy, 209 (2020) 568-575.
[14] X. Li, W. Liu, Z. Tang, T. Xu, J. Wang, Insight into dynamic interaction of molten MgCl2-NaCl-KCl with impurity water via FPMD simulations, Journal of Molecular Liquids, 314 (2020).
[15] G. Ciccotti, G. Jacucci, I.R. McDonald, Transport properties of molten alkali halides, Physical Review A, 13 (1976) 426-436.
[16] M.P. Tosi, F.G. Fumi, Ionic sizes and born repulsive parameters in the NaCl-type alkali halides—II: The generalized Huggins-Mayer form, Journal of Physics and Chemistry of Solids, 25 (1964) 45-52.
[17] W. Xie, J. Ding, G. Pan, Q. Fu, X. Wei, J. Lu, W. Wang, Heat and mass transportation properties of binary chloride salt as a high-temperature heat storage and transfer media, Solar Energy Materials and Solar Cells, 209 (2020).
[18] M. Wilson, P.A. Madden, Polarization effects in ionic systems from first principles, Journal of Physics: Condensed Matter, 5 (1993) 2687-2706.
[19] M. Salanne, P.A. Madden, Polarization effects in ionic solids and melts, Molecular Physics, 109 (2011) 2299-2315.
[20] J. Wu, H. Ni, W. Liang, G. Lu, J. Yu, Molecular dynamics simulation on local structure and thermodynamic properties of molten ternary chlorides systems for thermal energy storage, Computational Materials Science, 170 (2019).
[21] M. Salanne, B. Rotenberg, S. Jahn, R. Vuilleumier, C. Simon, P.A. Madden, Including many-body effects in models for ionic liquids, Theoretical Chemistry Accounts, 131 (2012) 1143.
[22] F. Wu, S. Roy, A.S. Ivanov, S.K. Gill, M. Topsakal, E. Dooryhee, M. Abeykoon, G. Kwon, L.C. Gallington, P. Halstenberg, B. Layne, Y. Ishii, S.M. Mahurin, S. Dai, V.S. Bryantsev, C.J. Margulis, Elucidating Ionic Correlations Beyond Simple Charge Alternation in Molten MgCl2–KCl Mixtures, The Journal of Physical Chemistry Letters, 10 (2019) 7603-7610.
[23] F. Wu, S. Sharma, S. Roy, P. Halstenberg, L.C. Gallington, S.M. Mahurin, S. Dai, V.S. Bryantsev, A.S. Ivanov, C.J. Margulis, Temperature Dependence of Short and Intermediate Range Order in Molten MgCl2 and Its Mixture with KCl, The Journal of Physical Chemistry B, 124 (2020) 2892-2899.

[24] K.T. Tang, J.P. Toennies, An improved simple model for the van der Waals potential based on universal damping functions for the dispersion coefficients, The Journal of Chemical Physics, 80 (1984) 3726-3741.
[25] Y. Ishii, S. Kasai, M. Salanne, N. Ohtori, Transport coefficients and the Stokes–Einstein relation in molten alkali halides with polarisable ion model, Molecular Physics, 113 (2015) 2442-2450.
[26] J. Lu, S. Yang, G. Pan, J. Ding, S. Liu, W. Wang, Thermal and Transport Properties of Molten Chloride Salts with Polarization Effect on Microstructure, Energies, 14 (2021).
[27] A. Marin-Laflèche, M. Haefele, L. Scalfi, A. Coretti, T. Dufils, G. Jeanmairet, S. Reed, A. Serva, R. Berthin, C. Bacon, S. Bonella, B. Rotenberg, P. Madden, M. Salanne, MetalWalls: A classical molecular dynamics software dedicated to the simulation of electrochemical systems, Journal of Open Source Software, 5 (2020).
[28] P.P. Ewald, Die Berechnung optischer und elektrostatischer Gitterpotentiale, Annalen der Physik, 369 (1921) 253-287.
[29] W.C. Swope, H.C. Andersen, P.H. Berens, K.R. Wilson, A computer simulation method for the calculation of equilibrium constants for the formation of physical clusters of molecules: Application to small water clusters, The Journal of Chemical Physics, 76 (1982) 637-649.
[30] S. Nosé, A unified formulation of the constant temperature molecular dynamics methods, The Journal of Chemical Physics, 81 (1984) 511-519.
[31] W.G. Hoover, Canonical dynamics: Equilibrium phase-space distributions, Physical Review A, 31 (1985) 1695-1697.
[32] G.J. Martyna, D.J. Tobias, M.L. Klein, Constant pressure molecular dynamics algorithms, The Journal of Chemical Physics, 101 (1994) 4177-4189.
[33] M. Brehm, B. Kirchner, TRAVIS - a free analyzer and visualizer for Monte Carlo and molecular dynamics trajectories, Journal of Chemical Information and Modeling, 51 (2011) 2007-2023.
[34] M.P. Allen, D.J. Tildesley, Computer simulatons of liquids, Oxford University Press (1987).
[35] T. Ikeshoji and B. Hafskjold, Non-equilibrium molecular dynamics calculation of heat conduction in liquid and through liquid-gas interface, Molecular Physics, 81 (1994) 251-261.
[36] F. Lantelme, P. Turq, B. Quentrec, J.W.E. Lewis, Application of the molecular dynamics method to a liquid system with long range forces (Molten NaCl), Molecular Physics, 28 (1974) 1537-1549.
[37] X. Wang, J.D. Rincon, P. Li, Y. Zhao, J. Vidal, Thermophysical Properties Experimentally Tested for NaCl-KCl-MgCl2 Eutectic Molten Salt as a Next-Generation High-Temperature Heat Transfer Fluids in Concentrated Solar Power Systems, Journal of Solar Energy Engineering, 143 (2021), 041005.
[38] X. Xu, G. Dehgani, J. Ning, P. Li, Basic properties of eutectic chloride salts NaCl-KCl-$ZnCl_2$ and NaCl-KCl-$MgCl_2$as HTFs and thermal storage media measured using simultaneous DSC-TGA, Solar Energy, 162 (2018), 432-441.
[39] C. Villada, W. Ding, A. Bonk, T. Bauer, Engineering molten MgCl2–KCl–NaCl salt for high-temperature thermal energy storage: Review on salt properties and corrosion control strategies, Solar Energy Materials and Solar Cells, 232 (2021), 111344.
[40] Y. Li, X. Xu, X. Wang, P. Li, Q. Hao, B. Xiao, Survey and evaluation of equations for thermophysical properties of binary/ternary eutectic salts from NaCl, KCl, MgCl2, CaCl2, ZnCl2 for heat transfer and thermal storage fluids in CSP, Solar Energy, 152 (2017) 57-79.
[41] Y. Nagasaka, N. Nakazawa, A. Nagashima, Experimental determination of the thermal diffusivity of molten alkali halides by the forced Rayleigh scattering method. I. Molten LiCl, NaCl, KCl, RbCl, and CsCl, International Journal of Thermophysics, 13 (1992) 555-574.

[42] Y. Ishii, K. Sato, M. Salanne, P.A. Madden, N. Ohtori, Thermal Conductivity of Molten Alkali Metal Fluorides (LiF, NaF, KF) and Their Mixtures, The Journal of Physical Chemistry B, 118 (2014) 3385-3391.
[43] G.J. Janz, II.C - METAL OXIDE-MOLTEN SALT SYSTEMS, in: G.J. Janz (Ed.) Molten Salts Handbook, Academic Press, 1967, pp. 116-117.
[44] J.O.M. Bockris, S.R. Richards, L. Nanis, Self-Diffusion and Structure in Molten Group II Chlorides1, The Journal of Physical Chemistry, 69 (1965) 1627-1637.